

**Eddy covariance mapping and quantification of surface CO₂ leakage
fluxes**

Jennifer L. Lewicki^{1*} and George E. Hilley²

^{1*}Earth Sciences Division, Ernest Orlando Lawrence Berkeley National Laboratory, 1
Cyclotron Rd., Berkeley, CA, 94720 USA, e-mail: jllewicki@lbl.gov, ph: 510-495-2818,
fax: 510-486-5686

²Department of Geological and Environmental Sciences, Stanford University, Stanford,
CA, 94305 USA

Abstract. We present eddy covariance measurements of net CO₂ flux (F_c) made during a controlled release of CO₂ (0.3 t d⁻¹ from 9 July to 7 August 2008) from a horizontal well ~100 m in length and ~2.5 m in depth located in an agricultural field in Bozeman, MT. We isolated fluxes arising from the release (F_{cr}) by subtracting fluxes corresponding to a model for net ecosystem exchange from F_c . A least-squares inversion of 611 F_{cr} and corresponding modeled footprint functions recovered the location, length, and magnitude of the surface CO₂ flux leakage signal, although high wavenumber details of the signal were poorly resolved. The estimated total surface CO₂ leakage rate (0.32 t d⁻¹) was within 7% of the release rate.

Keywords: Eddy covariance; Carbon dioxide flux; Least-squares inversion; Leakage; Volcano, geothermal, and geologic carbon storage monitoring

1. Introduction

Measurement of the spatial distribution and quantification of surface CO₂ emissions derived from volcanic, geothermal, and metamorphic (VGM) sources have been utilized for volcano and geothermal monitoring and estimation of the contribution of these emissions to the global carbon cycle [e.g., *Baubron et al.*, 1991; *Farrar et al.*, 1995; *Chiodini et al.*, 1998; *Chiodini et al.*, 1999; *Bergfeld et al.*, 2001; *Hernandez et al.*, 2001; *Notsu et al.*, 2006; *Werner and Cardellini*, 2006]. In addition, techniques with the ability to detect and characterize potential CO₂ leakage from storage reservoirs will be important for the monitoring and verification of geologic carbon sequestration (GCS) projects [e.g., *Oldenburg et al.*, 2003; *IPCC*, 2005]. Hereafter, we refer to surface CO₂ emissions from any of the afore-mentioned sources as CO₂ “leakage”.

The accumulation chamber (AC) method [e.g., *Chiodini et al.*, 1998] measures soil CO₂ flux on small spatial scales (cm²) and has been reliably used to map surface CO₂ leakage and quantify CO₂ emissions from VGM systems. Eddy covariance (EC), a micrometeorological technique traditionally used to measure net ecosystem exchange (*NEE*) under certain atmospheric and terrain conditions [e.g., *Baldocchi*, 2003], offers the benefit of an automated CO₂ flux measurement that does not interfere with the ground surface, is averaged over both time and space, and has a relatively large spatial scale (m²-km²). EC can reliably measure volcanic CO₂ fluxes [*Anderson and Farrar*, 2001; *Werner et al.*, 2000; 2003; *Lewicki et al.*, 2008], suggesting that the method has the potential to map the spatial distribution of surface CO₂ leakage fluxes and quantify total leakage rates

from geologic systems. While forward modeling has been used to predict atmospheric CO₂ concentrations resulting from both low density and dense gas leakage fluxes [Costa *et al.*, 2005; 2008], inverse modeling of EC CO₂ fluxes has only recently been used to predict surface CO₂ flux distributions [Lewicki *et al.*, 2009]. Lewicki *et al.* [2009] attempted to detect, locate, and quantify relatively small leakage flux signals within a background ecosystem at a field facility where CO₂ was released at controlled rates from a horizontal well in the shallow subsurface. The leakage signal was enhanced by removing fluxes that could be due to *NEE* and a least-squares inversion of a limited set (75) of measured EC CO₂ fluxes and modeled footprint functions was performed. While somewhat encouraging, the small number of observations and poor control on *NEE* resulted in coarse definition of the leakage signal and vast underestimation of its magnitude.

In the present contribution, we build on our previous work by using EC CO₂ flux measurements made during a recent controlled release of CO₂ at the same rate (0.3 t d⁻¹), but over a longer period (28 versus 8 days) than that measured by Lewicki *et al.* [2009]. We improved the filter that removes *NEE*, while avoiding loss of leakage signal. We perform a least-squares inversion of EC fluxes and modeled footprint functions to map the spatial distribution of surface fluxes. The surface leakage signal was accurately located and quantified (within 7% of the release rate) based on this approach. Results demonstrate the potential for EC to map and quantify CO₂ emissions from VGM systems and GCS sites under amenable atmospheric and terrain conditions.

2. Methods

The CO₂ release was conducted at Montana State University, Bozeman, MT. The field site was nearly flat, with vegetation composed mostly of prairie grasses and alfalfa and was mowed on 26-27 June 2008. A well was located in the field with a 70-m-long perforated and nearly horizontal section at its center and unperforated sections on its two sloping ends. The perforated section was located at 1.3 – 2.5 m depth and was divided into six zones separated by inflatable packers. From 9 July to 7 August 2008, 0.3 t CO₂ d⁻¹ (300 kg CO₂ d⁻¹) were released from the well, 39.0 kg CO₂ d⁻¹ from the far southwest perforated zone and 52.2 kg CO₂ d⁻¹ from each of the other five zones (see *Lewicki et al.* [2009] for additional field site information).

We measured soil CO₂ flux repeatedly on a grid at 2.5 to 10 m spacing (Figure 1) from 6 July to 2 August 2008 using the AC method. A soil CO₂ flux map was interpolated from grid measurements made on 25 July 2008 using a minimum curvature spline technique. Surface CO₂ leakage discharge (t d⁻¹) was estimated based on grid measurements as described in *Lewicki et al.* [2007].

We deployed an EC station 35 m northwest of the center of the release well from 12 June to 26 August 2008 (Figure 1). A Gill-Solent WindMaster Pro sonic three-dimensional anemometer/thermometer measured wind speeds in three orthogonal directions and sonic temperature at 10 Hz. A LI-COR LI-7500 open-path CO₂-H₂O infrared gas analyzer measured CO₂ and water vapor densities at 10 Hz. Both sensors were mounted atop a

tripod tower at 3.2 m height. Photosynthetically active radiation (PAR) was measured by a LI-COR LI-190SA quantum sensor at 2 m height every 5 s and averaged over 30 min.

Net CO_2 flux (F_c) was calculated for 30-minute periods as the temporal covariance of CO_2 density (c) and vertical wind velocity (w),

$$F_c = \overline{w'c'} \quad (1)$$

where the overbar denotes time averaging and primes denote fluctuations in w and c relative to their mean values. Coordinate rotation, WPL correction, raw signal de-spiking, and filtering F_c data according to stationarity and friction velocity criteria were applied as described in *Lewicki et al.* [2009].

The large variability of NEE may mask relatively small CO_2 flux leakage signals. *Lewicki et al.* [2009] estimated NEE according to:

$$NEE = -\left(\frac{F_{max} \alpha PAR}{\alpha PAR + F_{max}}\right) + R_{eco}, \quad (2)$$

where F_{max} is the maximum CO_2 flux at infinite light, α is the apparent quantum yield, and R_{eco} is ecosystem respiration [*Falge et al.*, 2001]. If F_{max} , α , and R_{eco} can be estimated, ecosystem fluxes can be removed from F_c to estimate residual F_c (F_{cr}) that may result from non-biologic sources [*Lewicki et al.*, 2009]. Our previous work

estimated R_{eco} by assuming it depends exponentially on soil temperature. Because this model was unable to uniquely distinguish between contemporaneous CO_2 leakage and R_{eco} effluxes, it tended to overestimate R_{eco} , resulting in removal of part of the leakage signal. To avoid this problem, this work estimates the photosynthetic uptake component of NEE (first term on right side of Equation (2)) as described by *Lewicki et al.*, [2009], but assumes that R_{eco} was constant during the observation period and equal to the average of background nighttime F_c values measured before and after the CO_2 release ($18 \text{ g m}^{-2} \text{ d}^{-1}$). F_{cr} values were then calculated by removing modeled NEE from the F_c time series.

Each EC flux measurement sources a particular area upwind of the sensors whose geometry depends on factors such as sensor height, atmospheric stability, and surface roughness. The footprint function, $f(x_m - x', y_m - y', z_m - z_0)$, describes the relationship between F_{cr} measured at point (x_m, y_m, z_m) and the distribution of source CO_2 fluxes at the surface from which ecological signals are removed ($Q_{cr}(x', y', z' = z_0)$):

$$F_{cr}(x_m, y_m, z_m) = \int_{-\infty}^{\infty} \int_{-\infty}^{\infty} Q_{cr}(x', y', z' = z_0) \cdot f(x_m - x', y_m - y', z_m - z_0) dx' dy' \quad (3)$$

[e.g., *Horst and Weil*, 1992; *Schmid*, 1997]. If the spatial distribution of Q_{cr} is relatively constant over time, changes in F_{cr} will divulge this distribution as the footprint function varies with atmospheric conditions [*Lewicki et al.*, 2009].

The Flux Source Area Model (FSAM) of *Schmid* [1997] was used to model footprint functions during the CO_2 release using the following inputs: (1) $z_m = 3.2 \text{ m}$; (2) surface

roughness height, $z_0 = 0.05$ m; (3) measured mean horizontal wind direction; (4) cross-wind turbulence near the surface (σ_v/u_* , where σ_v and u_* are the standard deviation of wind speed in the cross-wind direction and friction velocity, respectively); (5) calculated Monin-Obukhov length, L . We calculated f at the center of each 2.5 m x 2.5 m pixel in the model domain for each F_{cr} measured during the release. We averaged f at each point for the 611 footprints to reveal areas from which 50, 75, 90, and 95 % of the footprint weights were contained during the release time (Figure 1).

We model the spatial distribution of surface fluxes ($\overrightarrow{Q_{cr}}$) during the CO₂ release using a linear, least-squares inversion of 611 modeled footprint functions and observed $\overrightarrow{F_{cr}}$, following the methods described in *Lewicki et al.* [2009]. Since the area within ~75 m of the EC station contributed to 90% of F_{cr} measured during the CO₂ release (Figure 1), the model domain was selected as 150 x 150 m. Often in such inversions, the best-fit modeled $\overrightarrow{Q_{cr}}$ shows large point-to-point oscillations, producing a rough solution that is physically unrealistic. To ameliorate these effects, we apply a finite-difference approximation of curvature between each of the adjacent $\overrightarrow{Q_{cr}}$ values that is minimized along with the misfit between observed and modeled $\overrightarrow{F_{cr}}$ [e.g., *Harris and Segall*, 1987]. The modeled $\overrightarrow{Q_{cr}}$ distribution is a compromise between the constraints provided by observations versus those that require a spatially smooth solution, the relative influence of which is controlled by the weight (w_{sm}) applied to the curvature finite difference approximation. By systematically changing the value of w_{sm} , we can determine values of this parameter that result in the greatest decrease in the solution roughness that does not

necessitate a correspondingly large change in the data misfit (see *Lewicki et al.* [2009] for detailed discussion).

3. Results

The surface CO₂ flux leakage signal measured by the AC method was expressed as six point sources of elevated CO₂ flux, aligned along the surface trace of the well (Figure 1).

The CO₂ leakage discharge estimated based on these measurements was 0.31 t d⁻¹.

A shift upwards in F_c values occurred after the field was mowed due to a decrease in plant leaf area and photosynthetic uptake (Figure 2a). Elevated F_c values were measured during the CO₂ release, relative to the time prior to and after the release. The mean and standard deviation of the F_c time series were -18.9 and 31.6 g m⁻² d⁻¹, respectively. The mean and standard deviation of F_{cr} time series were 1.9 and 15.0 g m⁻² d⁻¹, respectively; NEE subtraction thus removed the negative bias from and decreased the variability of fluxes, while preserving elevated values during the release (Figure 2b). During the release, relatively high F_{cr} was typically measured when the EC station was located down wind of the well (mean horizontal wind direction ~90-180°; Figure 2c).

We conducted checkerboard tests to assess the ability of the inversion to resolve \vec{Q}_{cr} features of different spatial scales within the model domain. A $w_{sm} = 1$ was used in the inversions because it provided the optimal compromise between spatial continuity across the model solution space and misfit between measured and modeled F_{cr} .

(Supplement 1a). Checkerboards were assigned alternating patches of low and high Q_{cr} with dimensions of 25 x 25, 50 x 50, and 75 x 75 m (Supplement 2a, c, and e, respectively). A given checkerboard was weighted by each of the 611 footprint functions modeled during the CO₂ release (Equation 3), to yield 611 synthetic F_{cr} values.

Randomly distributed noise with the mean and standard deviation of $\overrightarrow{F_{cr}}$ measured during the release was added to the synthetic $\overrightarrow{F_{cr}}$. The spatial distribution of $\overrightarrow{Q_{cr}}$ was then modeled by inversion of the synthetic $\overrightarrow{F_{cr}}$ and footprint functions (Supplement 2b, d, and f). Results indicate that 25 x 25, 50 x 50 and 75 x 75 m $\overrightarrow{Q_{cr}}$ patches centered within ~ 18, 35, and 53 m, respectively, of the EC station were recoverable, while 25 x 25 and 50 x 50 m patches centered at greater distances from the EC station were unrecoverable (Supplement 2).

Figure 3 shows maps of $\overrightarrow{Q_{cr}}$ modeled based on inversion of the measured $\overrightarrow{F_{cr}}$ and modeled footprint functions during the CO₂ release using $w_{sm} = 0.31, 1.0, \text{ and } 3.2$. For each of the inversions, an area of relatively high $\overrightarrow{Q_{cr}}$ with the approximate length of, but greater width than the surface CO₂ flux leakage signal observed in Figure 1 is present near the surface trace of the well. With increasing w_{sm} , the $\overrightarrow{Q_{cr}}$ anomaly magnitude decreases, while its geometry becomes rounder and its center moves closer to the well trace. Surface CO₂ leakage discharges, estimated by integrating $\overrightarrow{Q_{cr}}$ values over the model domain, were 0.40, 0.32, and 0.23 t d⁻¹ for $w_{sm} = 0.32, 1, \text{ and } 3.2$, respectively (Figure 3). Supplement 1b shows the decrease in leakage discharge with increasing w_{sm} .

4. Discussion and Conclusions

We present an example of inversion of measured EC CO₂ fluxes and modeled footprint functions to both map the spatial distribution of and accurately quantify surface CO₂ fluxes derived from subsurface CO₂ leakage. The map of modeled \overrightarrow{Q}_{cr} ($w_{sm} = 1$) indicated the presence of CO₂ leakage from an area of similar length to, and nearly centered on the surface trace of the horizontal well (Figure 3b). Also, assuming that the 0.3 t CO₂ d⁻¹ released from the well was emitted at the surface, EC estimated the surface CO₂ leakage discharge within 7%, based on modeled \overrightarrow{Q}_{cr} (Figure 3b). Furthermore, the leakage discharge estimated based on EC measurements (0.32 t d⁻¹) compared closely to that estimated based on AC measurements (0.31 t d⁻¹).

The choice of w_{sm} used in the inversion affects both the spatial distribution and magnitude of the modeled CO₂ leakage signal. With increasing w_{sm} , smoothing dominates over data misfit in the inversion yielding a smoother and lower magnitude \overrightarrow{Q}_{cr} distribution (Supplement 1 and Figure 3). A w_{sm} providing the optimal compromise between spatial continuity across the model solution space and misfit between measured and modeled \overrightarrow{F}_{cr} should therefore be selected to yield the most accurate mapping and quantification of CO₂ leakage (e.g., Figure 3b).

As demonstrated by checkerboard resolution tests (Supplement 2), inversion of the \overrightarrow{F}_{cr} and footprint functions available to us during the CO₂ release should be able to recover a \overrightarrow{Q}_{cr} signal with a spatial scale on the order of ≥ 50 m located at the distance of the release well from the EC station (35 m), while \overrightarrow{Q}_{cr} features of smaller scale will be difficult to

recover. The maps of modeled $\overline{Q_{cr}}$ therefore showed leakage signals of similar length to that observed in Figure 1, but were unable to reproduce the narrow width of the measured leakage CO₂ flux anomaly. Inversion resolution could be improved if multiple EC stations are deployed in different locations or an array of EC sensors is installed at more than one height at a given location and repeatedly sample a leakage area with different flux footprints. However, the AC method will likely remain the most effective tool for detailed mapping of small-scale heterogeneities in surface CO₂ fluxes.

Based on inversion of EC observations, *Lewicki et al.* [2009] roughly located a CO₂ leakage signal of similar magnitude and geometry to that investigated in the present study, while they underestimated the CO₂ leakage discharge by 93%. Our results improve upon those of *Lewicki et al.* [2009] with respect to both mapping and quantification of $\overline{Q_{cr}}$, likely because (1) a larger data set was available for the inversion (611 versus 75 F_{cr} measurements) and (2) estimation of R_{eco} based on average background nighttime F_c minimized loss of CO₂ leakage signal in F_{cr} calculations. R_{eco} estimation in future studies could be improved by concurrent AC and/or EC measurements of CO₂ fluxes in background areas away from, but with similar ecosystem characteristics as the area under investigation for CO₂ leakage. Furthermore, estimation of NEE and its removal from F_c may not be necessary in many VGM areas where geologic leakage fluxes dominate over ecosystem fluxes. Our results suggest that EC may have significant utility for mapping and quantification of surface CO₂ emissions derived from leakage from natural geologic sources and GCS sites.

Acknowledgements. We thank G. Chiodini and D. Vasco for valuable manuscript review, L. Dobeck and K. Gullickson for assistance in the field, and H.P. Schmid for the FSAM source code. This work was funded by the ZERT Project, Assistant Secretary for Fossil Energy, Office of Sequestration, Hydrogen, and Clean Coal Fuels, NETL, of the U.S. Dept. of Energy under Contract No. DE-AC02-05CH11231.

References

- Anderson, D.E. and C.D. Farrar (2001), Eddy covariance measurement of CO₂ flux to the atmosphere from an area of high volcanogenic emissions, Mammoth Mountain, California. *Chem. Geol.*, 177, 31–42.
- Baldocchi, D.D. (2003), Assessing the eddy covariance technique for evaluating carbon dioxide exchange rates of ecosystems: past, present, and future. *Global Change Biol.*, 9, 479–492.
- Baubron, J.-C., P. Allard, J.-C. Sabroux, D. Tedesco, and J.P. Toutain, (1991), Soil gas emanations as precursory indicators of volcanic eruptions. *J. Geol. Soc.*, 148, 571–576.
- Bergfeld, D., F. Goff, and C.J. Janik (2001), Elevated carbon dioxide flux at the Dixie Valley geothermal field, Nevada; relations between surface phenomena and the geothermal reservoir. *Chem. Geol.*, 177, 43–66.
- Chiodini, G., G.R. Cioni, M. Guidi, B. Raco, and L. Marini (1998), Soil CO₂ flux measurements in volcanic and geothermal areas. *Appl. Geochem.*, 13, 543–552.
- Chiodini, G., F. Frondini, D.M. Kerrick, J. Rogie, L. Peruzzi, and A.R. Zanzari (1999), Quantification of deep CO₂ fluxes from central Italy. Examples of carbon balance for regional aquifers and of soil diffuse degassing. *Chem. Geol.* 159, 205–222.
- Costa, A., G. Macedonio, and G. Chiodini (2005), Numerical model of gas dispersion emitted from volcanic sources, *Annals Geophys.*, 48, 4/5.
- Costa A., G. Chiodini, D. Granieri, A. Folch, R.K.S. Hankin, S. Caliro, C. Cardellini, and R. Avino (2008), A shallow layer model for heavy gas dispersion from natural

- sources: application and hazard assessment at Caldara di Manziana, Italy. *Geochem. Geophys. Geosyst.*, 9, Q03002, doi:10.1029/2007GC001762.
- Falge, E., D.D. Baldocchi, R.J. Olson, et al. (2001), Gap filling strategies for defensible annual sums of net ecosystems exchange. *Agric. For. Meteorol.* 107, 43–69.
- Farrar, C.D., M.L. Sorey, W.C. Evans, J.F. Howle, B.D. Kerr, B.M. Kennedy, Y. King, and J.R. Southon (1995), Forest-killing diffuse CO₂ emission at Mammoth Mountain as a sign of magmatic unrest. *Nature*, 376, 675–678.
- Harris, R., and P. Segall (1987), Detection of a locked zone at depth on the Parkfield, California segment of the San Andreas fault. *J. Geophys. Res.*, 92, 27945–27962.
- Hernandez, P.A., K. Notsu, J.M. Salazar, T. Mori, G. Natale, H. Okada, G. Virgilli, Y. Shimoike, M. Sato, and N.M. Perez (2001), Carbon dioxide degassing by advective flow from Usu volcano, Japan. *Science*, 2001, 83–86.
- Horst, T.W. and J.C. Weil (1992), Footprint estimation for scalar flux measurements in the atmospheric surface-layer. *Bound. Layer Meteorol.*, 59, 279–296.
- IPCC (2005), IPCC Special Report on Carbon Dioxide Capture and Storage, Cambridge University Press, Cambridge.
- Lewicki, J.L., C.M. Oldenburg, L. Dobeck, L. and L. Spangler (2007), Surface CO₂ leakage during two shallow subsurface CO₂ releases. *Geophys. Res. Lett.*, 34, L24402, doi:101029/2007GL032047.
- Lewicki, J. L., M.L. Fischer, and G.E. Hilley (2008), Six-week time series of eddy covariance CO₂ flux at Mammoth Mountain, California: performance evaluation and role of meteorological forcing. *J. Volcanol. Geotherm. Res.*, 171, 178–190.

- Lewicki, J.L., G.E. Hilley, M.L. Fischer, L. Pan, C.M. Oldenburg, L. Dobeck, and L. Spangler (2009), Eddy covariance observations of surface leakage during shallow subsurface CO₂ releases. *J. Geophys. Res.*, *114*, D12302, doi:10.1029/2008JD011297.
- Notsu, K., K. Sugiyama, M. Hosoe, A. Uemura, Y. Shimolke, F. Tsunomori, H. Sumino, J. Yamamoto, T. Mori, and P.A. Hernandez (2005), Diffuse CO₂ efflux from Iwojima volcano, Izu-Ogasawara arc, Japan. *J. Volcanol. Geotherm. Res.*, *139*, 147-161.
- Oldenburg, C.M., J.L. Lewicki, and R.P. Hepple (2003), Near-surface monitoring strategies for carbon dioxide storage verification, *Lawrence Berkeley National Laboratory Report LBNL-54089*.
- Schmid, H.P. (1997), Experimental design for flux measurements: matching scales of observations and fluxes. *Agri. For. Meteorol.*, *87*, 179–200.
- Werner, C. and C. Cardellini (2006), Comparison of carbon dioxide emissions with fluid upflow, chemistry, and geologic structures at the Rotorua geothermal system, New Zealand. *Geothermics*, *35*, 221–238.
- Werner, C., G. Chiodini, D. Voigt, S. Caliro, R. Avino, M. Russo, T. Brombach, J. Wyngaard, and S. Brantley (2003), Monitoring volcanic hazard using eddy covariance at Solfatara volcano, Naples, Italy. *Earth Planet. Sci. Lett.*, *210*, 561–577.

Figure Captions

Figure 1. Map of log soil CO₂ flux, interpolated based on measurements made at the black dots on 25 July 2008. White line and black square show locations of surface trace of CO₂ release well and EC station, respectively. Mean EC flux 50, 75, 90, and 95% source area isopleths are shown for the CO₂ release time.

Figure 2. Time series of (a) F_c and (b) F_{cr} . 611 F_{cr} values used in the inversion are circled. Dashed lines and gray zones show timing of mowing of the field and CO₂ release, respectively. (c) Plot of F_{cr} versus wind direction measured during the CO₂ release.

Figure 3. Maps of modeled $\overline{Q_{cr}}$ for $w_{sm} =$ (a) 0.32, (b) 1.0, and (c) 3.2. White lines and squares show locations of surface trace of CO₂ release well and EC station, respectively.

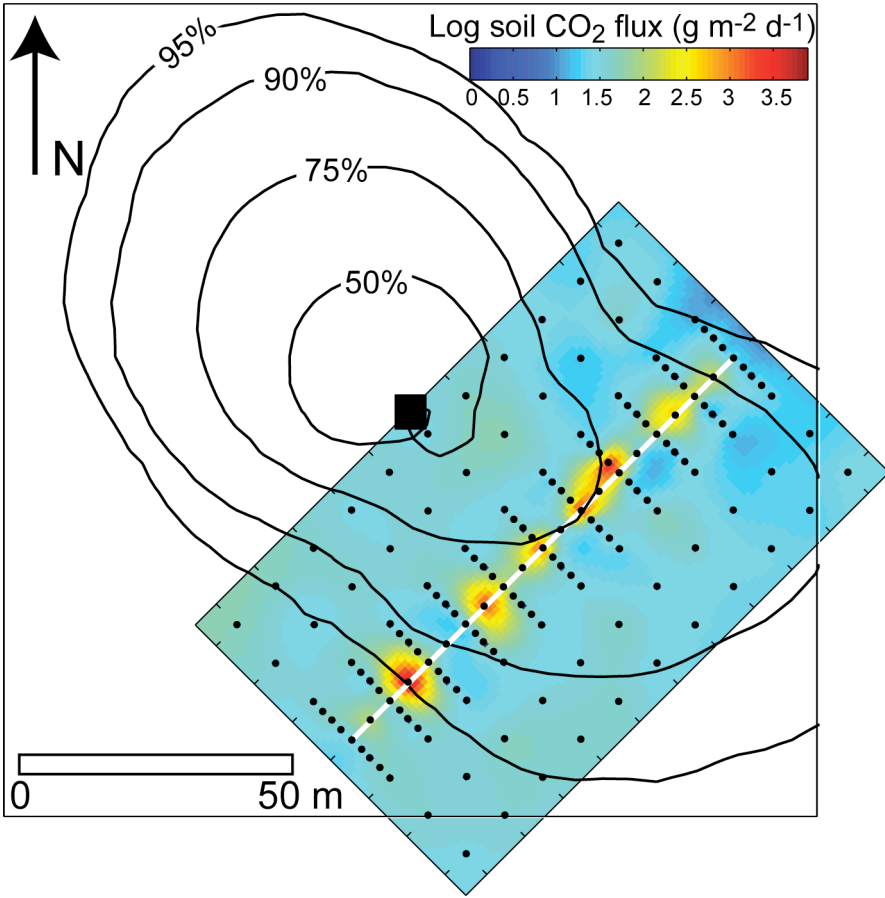


Figure 1

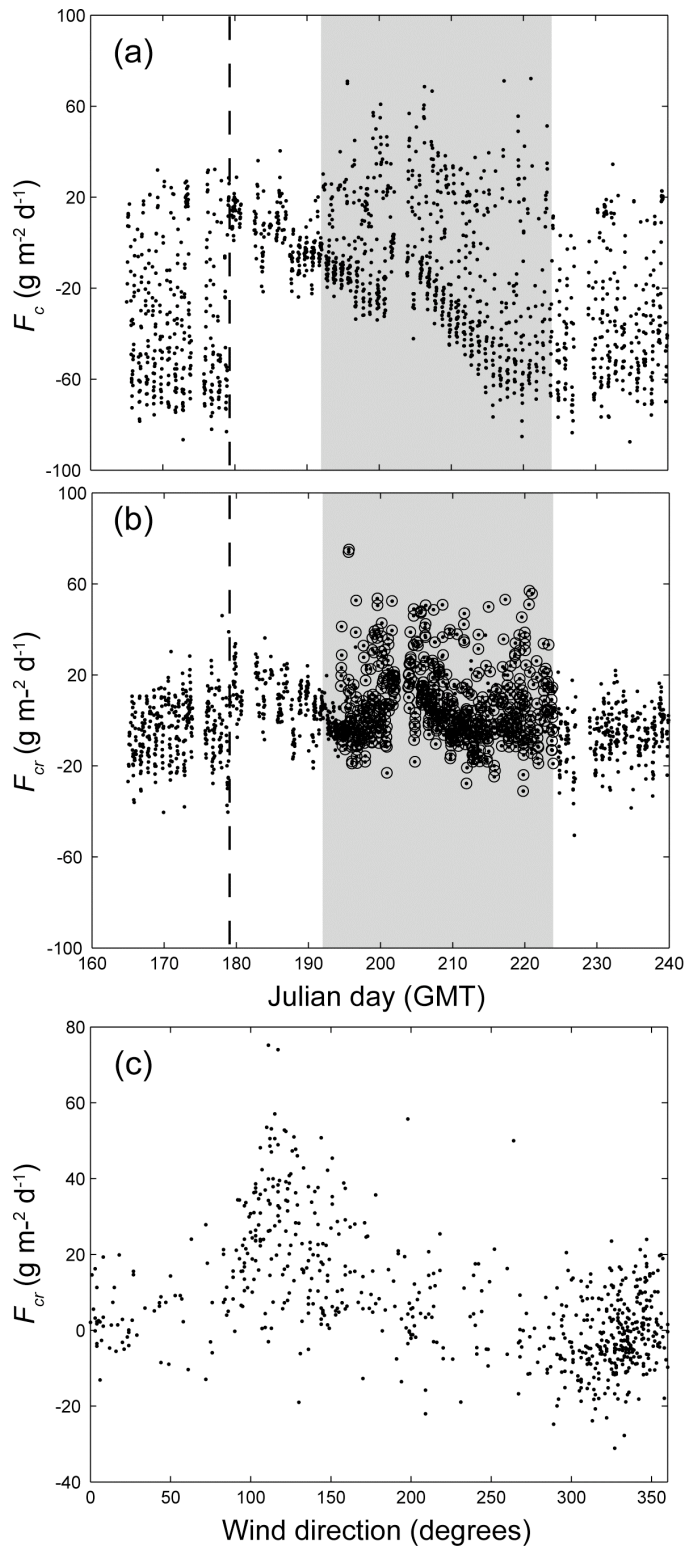
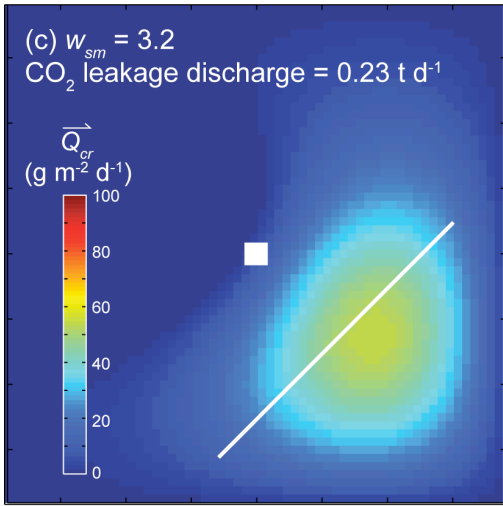
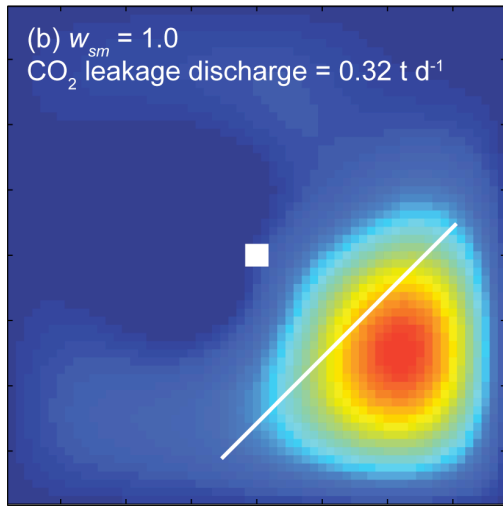
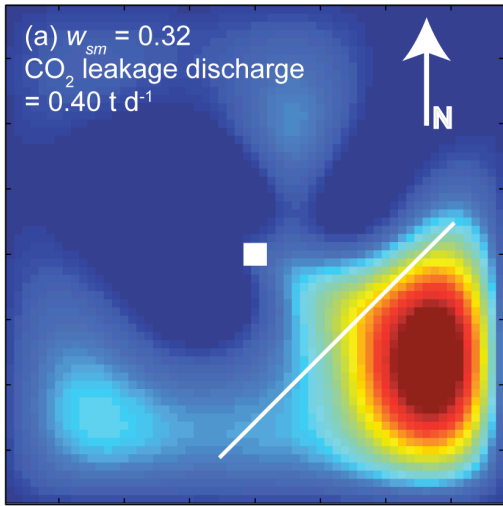


Figure 2



0 50 m

Figure 3